

Vinblastine resets tumor-associated macrophages toward M1 phenotype and promotes antitumor immune response

Yi-Na Wang,¹ Yuan-Yuan Wang,¹ Jin Wang,¹ Wen-Juan Bai,¹ Nai-Jun Miao,^{1,2} Jing Wang ^{1,2}

To cite: Wang Y-N, Wang Y-Y, Wang J, *et al.* Vinblastine resets tumor-associated macrophages toward M1 phenotype and promotes antitumor immune response. *Journal for ImmunoTherapy of Cancer* 2023;11:e007253. doi:10.1136/jitc-2023-007253

► Additional supplemental material is published online only. To view, please visit the journal online (<http://dx.doi.org/10.1136/jitc-2023-007253>).

Accepted 15 August 2023

ABSTRACT

Background Massive tumor-associated macrophage (TAM) infiltration is observed in many tumors, which usually display the immune-suppressive M2-like phenotype but can also be converted to an M1-like antitumor phenotype due to their high degree of plasticity. The macrophage polarization state is associated with changes in cell shape, macrophage morphology is associated with activation status. M1 macrophages appeared large and rounded, while M2 macrophages were stretched and elongated cells. Manipulating cell morphology has been shown to affect the polarization state of macrophages. The shape of the cell is largely dependent on cytoskeletal proteins, especially, microtubules. As a microtubule-targeting drug, vinblastine (VBL) has been used in chemotherapy. However, no study to date has explored the effect of VBL on TAM shape changes and its role in tumor immune response.

Method We used fluorescent staining of the cytoskeleton and quantitative analysis to reveal the morphological differences between M0, M1, M2, TAM and VBL-treated TAM. Flow cytometry was used to confirm the polarization states of these macrophages using a cell surface marker-based classification. In vivo antibody depletion experiments in tumor mouse models were performed to test whether macrophages and CD8⁺ T cell populations were required for the antitumor effect of VBL. VBL and anti-PD-1 combination therapy was then investigated in comparison with monotherapy. RNA-seq of TAM of treated and untreated with VBL was performed to explore the changes in pathway activities. siRNA mediated knockdown experiments were performed to verify the target pathway that was affected by VBL treatment.

Results Here, we showed that VBL, an antineoplastic agent that destabilizes microtubule, drove macrophage polarization into the M1-like phenotype both in vitro and in tumor models. The antitumor effect of VBL was attenuated in the absence of macrophages or CD8⁺ T cells. Mechanistically, VBL induces the activation of NF-κB and Cyba-dependent reactive oxygen species generation, thus polarizing TAMs to the M1 phenotype. In parallel, VBL promotes the nuclear translocation of transcription factor EB, inducing lysosome biogenesis and a dramatic increase in phagocytic activity in macrophages.

Conclusions This study explored whether manipulating cellular morphology affects macrophage polarization and consequently induces an antitumor response. Our data reveal a previously unrecognized antitumor mechanism of

WHAT IS ALREADY KNOWN ON THIS TOPIC

⇒ Recent studies showed that the phenotype of tumor associated macrophages (TAMs) is controlled by cell morphology. As a microtubule-targeting chemotherapeutic drug, the effect of vinblastine (VBL) on the TAM morphology and phenotype control as well as the role in tumor immune response have not been reported yet.

WHAT THIS STUDY ADDS

⇒ Here, we showed that the antitumor efficacy of VBL requires macrophages in mouse tumor model. Mechanistically, VBL resets TAM toward M1 phenotype through upregulating cyba expression and promoting reactive oxygen species generation. VBL also induces lysosome biogenesis and promotes phagocytic activity in macrophages.

HOW THIS STUDY MIGHT AFFECT RESEARCH, PRACTICE OR POLICY

⇒ This study reveals a different in vivo mechanism of action of a commonly used chemotherapy drug, and provides a rational to design combinations of VBL with immunotherapies to achieve enhanced antitumor immunity.

VBL and suggest a drug repurposing strategy combining VBL with immune checkpoint inhibitors to improve malignant tumor immunotherapy.

INTRODUCTION

Macrophages are among the most common cells in the colorectal and pulmonary tumor microenvironment,^{1–4} but their dynamic changes in the course of immunotherapy are incompletely understood.⁵ Macrophages infiltrating the tumor microenvironment are recognized as tumor-associated macrophages (TAMs). At the tumor initiation stage, TAMs create an inflammatory microenvironment that can induce mutation and promote tumor proliferation. However, TAMs promote angiogenesis, enhance tumor cell migration and invasion, and inhibit antitumor immune response during tumor progression.^{6,7} TAMs



© Author(s) (or their employer(s)) 2023. Re-use permitted under CC BY-NC. No commercial re-use. See rights and permissions. Published by BMJ.

¹Shanghai Institute of Immunology, Department of Immunology and Microbiology, Shanghai Jiao Tong University School of Medicine, Shanghai, China

²Center for Immune-related Diseases at Shanghai Institute of Immunology, Ruijin Hospital, Shanghai Jiao Tong University School of Medicine, Shanghai, China

Correspondence to

Dr Jing Wang;
jingwang@shsmu.edu.cn

are generally believed to promote tumor growth and metastasis.^{8,9} These immune cells also contribute to the formation of the immunosuppressive microenvironment and promote tumor immune escape and therapy resistance.^{10,11} Studies have demonstrated that TAM inhibits the efficacy of anticancer drugs, such as immune checkpoint blocking therapy, and increased TAM infiltration is often strongly related to poor prognosis or tumor progression in many types of solid tumors.^{12,13}

Mature macrophages typically exhibit one of two phenotypes, including the classically activated (M1-like) and alternatively activated macrophages (M2-like). TAMs usually display the M2-like phenotype, which accelerates the development and metastasis of tumors by forming an immunosuppressive microenvironment.¹⁴ Research has shown that M1-like macrophages can activate cytotoxic T lymphocytes by antigen presentation or secretion of proinflammatory cytokines, resulting in T cell proliferation and IFN γ secretion. Therefore, M1 TAMs are considered tumor-suppressive macrophages.¹⁵ Notably, macrophages are highly plastic cells and can undergo marked changes in their function. Therapeutic approaches under development aim to re-educate TAMs for antitumor immunity to increase tumor cell phagocytosis.

Cellular morphology has recently gained growing attention as a robust comprehensive biomarker of cell function.^{16,17} According to previous observations in both murine¹⁸ and human studies,¹⁹ macrophage morphology is associated with activation status; M1 macrophages appeared large and rounded, while M2 macrophages were stretched and elongated cells.²⁰ Manipulating cell morphology has been shown to affect the polarization state of macrophages. McWhorter *et al* succeeded in polarizing murine bone marrow-derived macrophages (BMDMs) toward an M2 phenotype by inducing the cells to an elongated morphology on micropatterned grooves with a width of 20 μ m.¹⁸ The shape of the cell is largely dependent on three groups of cytoskeletal protein filaments: microtubules, intermediate filaments, and actin filaments. Disrupting microtubules has been shown to induce changes in both cell shape and cell volume in macrophage cell lines.²¹ Cao *et al* found that microtubule inhibitor cabazitaxel promotes macrophages polarization toward M1 state through NF- κ B signaling activation, and thus enhancing the elimination of triple-negative breast cancer cells.²² These results show that targeting macrophages is a promising and effective strategy for tumor treatment. Other drugs that target microtubules have been used as antitumor chemotherapy agents, but their role and mechanism of actions in modulating tumor immune response is still in the beginning stage, and hence need further research.

The current study explored whether controlling macrophage morphology could trigger alterations in activation status and cellular responses in the context of tumors. We demonstrated that vinblastine (VBL), an antineoplastic drug that targets microtubule depolymerization, display antitumor effect by resetting TAMs from the

M2 phenotype to the proinflammatory M1 phenotype. Furthermore, VBL was shown to reprogram TAMs by activating the NF- κ B-Cyba axis to induce reactive oxygen species (ROS) generation, which is responsible for the phenotype conversion of macrophages. In addition, VBL dramatically increased the phagocytosis function of macrophages by promoting lysosome biogenesis. Collectively, our findings define a novel immunomodulatory mechanism of action of VBL for cancer treatment.

RESULTS

VBL reprograms TAMs toward antitumor M1-like phenotype and activates T cells

Murine bone marrow cells were first differentiated into mature M0 macrophages and then induced to the M1 phenotype with LPS+IFN γ or the M2 phenotype with IL-4 to examine the correlation of morphology to macrophage polarization states. Fluorescent staining of the cytoskeleton revealed significant morphological differences between the three kinds of macrophages, showing elongated projections in M2-like macrophages as opposed to a round and flattened morphology in M1-like macrophages (figure 1A). Flow cytometry analysis further confirmed the polarization states of these macrophages using a cell surface marker-based classification (figure 1B). BMDMs were treated with tumor cell conditioned medium (CM) to better mimic the tumor environment *in vivo*. Subsequently, the polarization spectrum of TAMs induced by different tumor cell CM was assessed using gene sets responsible for defining macrophage polarization states. The results revealed that M1 marker genes expression was increased, while the expression of M2 marker genes was decreased in VBL-treated TAM when compared with untreated TAM (online supplemental figure 1A,B). The *in vitro*-induced TAMs were treated with three microtubule-targeting drugs, VBL, colchicine, and paclitaxel. All three drugs could transform elongated TAMs into a round and flattened morphology similar to the M1-like phenotype (figure 1C). Flow cytometry analysis revealed that all three drugs had similar effects on inducing M1 polarization and inhibiting M2 polarization (figure 1D).

TAMs play a major role in immunosuppression by releasing immunomodulatory factors, such as PGE2, IL-10, and TGF β , which inhibit the cytotoxic activity of CD8⁺ T cells. Therefore, the effect of the three drugs on CD8⁺ T cell activation was investigated by treating macrophages. Cell proliferation dye-labeled CD8⁺ T cells were co-cultured with M0 macrophages or TAMs under different treatments. Co-culture with M0 or classically activated M1 macrophages (LPS+IFN γ induced) showed little effect on T cell proliferation (figure 1E,F). As expected, TAMs displayed a profound immunosuppressive effect with almost 100% suppression of T cell proliferation. However, only VBL treatment reversed the immunosuppressive effects of TAMs, while the other two drugs did not (figure 1E,F). Both MC38-CM-induced (M-induced) and LLC-CM-induced (L-induced) TAMs almost

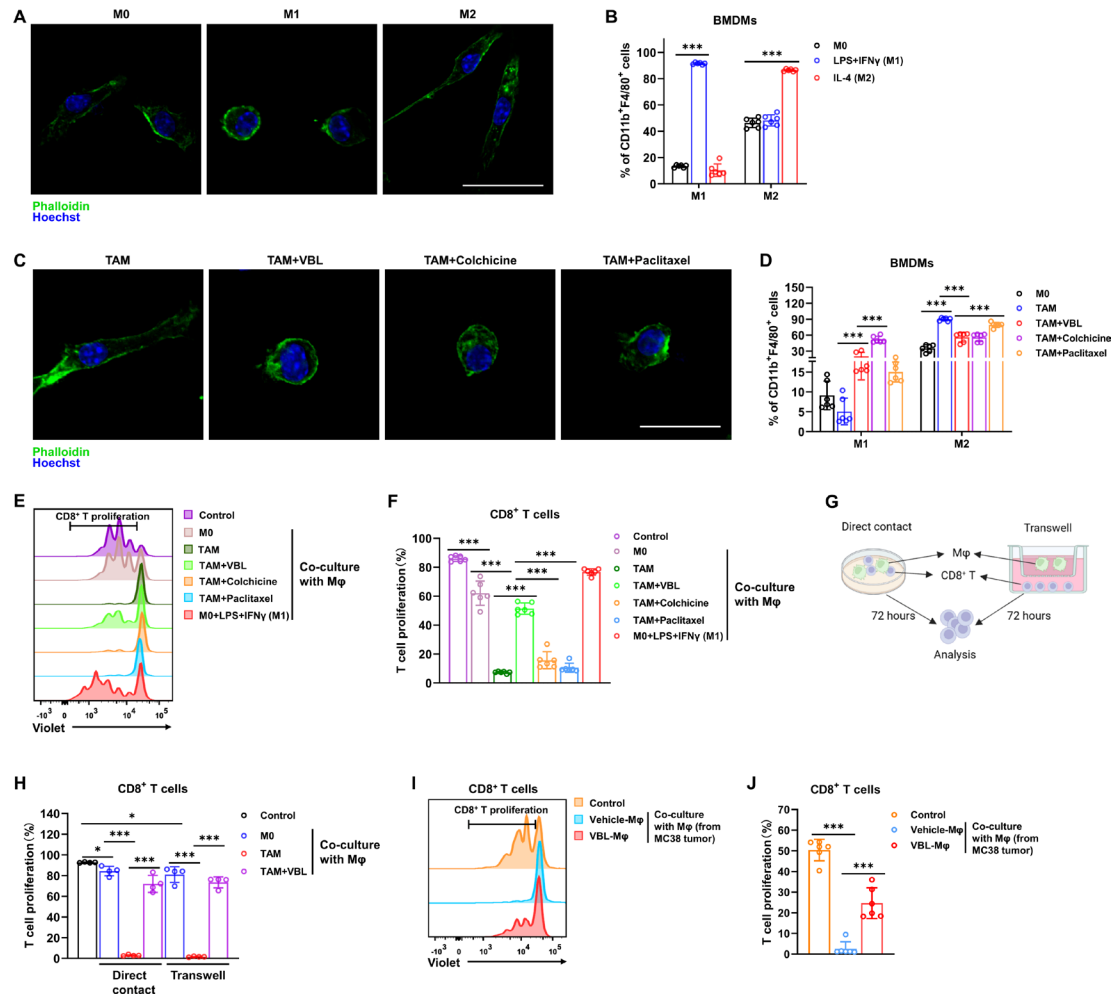


Figure 1 VBL reprograms TAMs toward the antitumor M1-like phenotype and activates T cells. (A) Immunostaining of M0, M1 (LPS+IFN γ induced), and M2 (IL-4 induced) macrophages with phalloidin and Hoechst. Scale bar: 20 μ m. (B) Flow cytometry analysis for M1 (F4/80 $^{+}$ CD11b $^{+}$ CD86 $^{+}$) and M2 (F4/80 $^{+}$ CD11b $^{+}$ CD206 $^{+}$) percentages in BMDMs under different treatments for 24 hours. n=6. (C) Immunostaining with phalloidin and Hoechst showed morphological changes in TAM following different treatments for 24 hours. Scale bar: 20 μ m. (D) Flow cytometry analysis for M1 (F4/80 $^{+}$ CD11b $^{+}$ CD86 $^{+}$) and M2 (F4/80 $^{+}$ CD11b $^{+}$ CD206 $^{+}$) percentage in BMDMs following their respective treatments for 24 hours. n=6. (E) Representative flow cytometry results of T cell proliferation after co-culture with M ϕ for 72 hours. (F) Statistical results of T cell proliferation in panel (E). n=6. (G) Schematic workflow for macrophage and T cell co-culture by direct contact or transwell. (H) T cell proliferation ratio after co-culture with macrophages by direct contact or transwell. n=4. (I) Representative flow cytometry results of T cell proliferation after co-culture with macrophages sorted from MC38 tumors for 72 hours. (J) Statistical results of T cell proliferation in panel (I). n=6. Data are presented as mean \pm SD. P values were determined by a two-tailed Student's t-test. *p<0.05, ***p<0.001. TAM, tumor-associated macrophage; VBL, vinblastine.

completely suppressed CD8 $^{+}$ T cell activation, whereas VBL-treated TAMs greatly restored CD8 $^{+}$ T cell proliferation (online supplemental figure 1C,D). Furthermore, transwells were used to separate macrophages and CD8 $^{+}$ T cells to examine whether the immunosuppressive function of TAMs required cell-cell contact (figure 1G). The inhibition efficiency of cells co-cultured in transwell was comparable to those co-cultured in direct contact, and VBL treatment significantly restored CD8 $^{+}$ T cell activation regardless of whether there was direct contact or not (figure 1H). In addition, macrophages sorted and purified from MC38 and LLC tumors in mice also displayed profound immunosuppressive effects, and macrophages purified from VBL-treated tumor-bearing mice also

restored CD8 $^{+}$ T cell activation (figure 1I,J, online supplemental figure 1E,F). Since CD69 is rapidly induced and transiently expressed on activated T and natural killer (NK) cells, we next detected the changes of CD69 in these cells using flow cytometry. CD8 $^{+}$ T cells sorted from tumor in vivo with VBL treatment have a higher CD69 expression level, indicating that VBL administration to tumor bearing mice can indeed activate CD8 $^{+}$ T cells within the tumor (online supplemental figure 1G). To exclude the possible direct impact of VBL on T cells or NK cells, we treat CD8 $^{+}$ T cells or NK cells with VBL directly. Results indicated that VBL cannot directly activate T cells or NK cells (online supplemental figure 1H,I), suggesting the indispensable role of macrophages in the indirect

activation of T cells by VBL. The above results indicated that, at least under these experimental conditions, TAMs suppress T cell proliferation mainly through secretory factors, which can be reversed by VBL treatment.

VBL-mediated antitumor effect is dependent on macrophages and CD8⁺ T cells

Although the antitumor effect of VBL has been attributed to its direct cytotoxicity for tumor cells, our in vitro findings suggested that VBL could re-educate TAMs and reverse its immunosuppressive function. To test whether VBL's anti-tumor effect requires immune activation, we established MC38 or LLC subcutaneously injected tumor models. VBL

treatment could suppress primary tumor growth in both models (figure 2A, online supplemental figure 2A). After VBL monotherapy, the percentage of TAMs (figure 2B, online supplemental figure 2B) was decreased in both tumor models, and the M1 cell percentage was increased, while the M2 cells decreased (figure 2C, online supplemental figure 2C). Meanwhile, the percentage of CD8⁺ T cell infiltration in tumors was also increased (figure 2D, online supplemental figure 2D). Gene expression analysis of macrophages purified from tumors revealed increased expression of M1 genes, while the expression of M2 genes was decreased after VBL treatment (figure 2E).

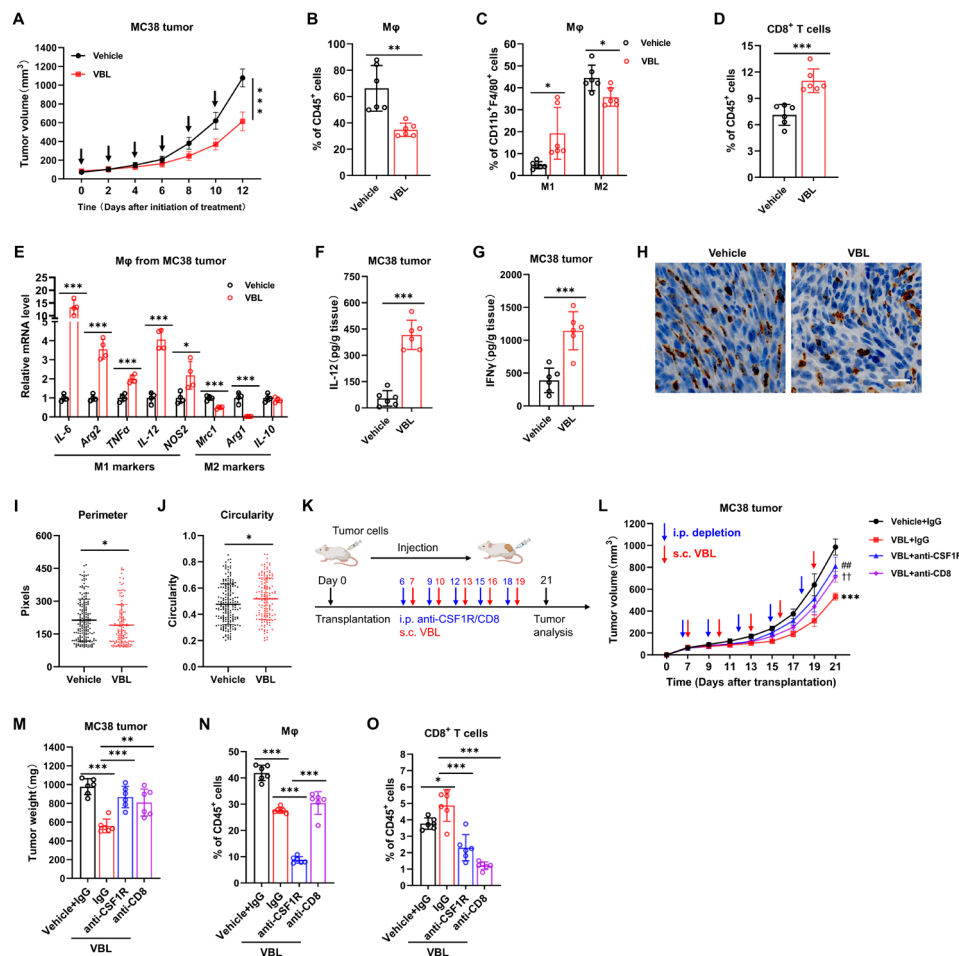


Figure 2 VBL-mediated antitumor effect is dependent on macrophages and CD8⁺ T cells. (A) Growth curve of MC38 tumor with and without VBL treatment (1.25 mg/kg weight, every other day), arrows indicate the treatment time. n=6. (B–D) Flow cytometry analysis for total macrophages (B), M1 or M2 cells (C), and T cells (D) in MC38 tumors with or without VBL treatment. n=6. (E) Gene expression of IL-6, Arg2, TNF α , IL-12, NOS2, Mrc1, Arg1, and IL-10 in macrophages sorted from MC38 tumors. n=4. (F–G) ELISA analysis of IL-12 (F) and IFN γ (G) levels in MC38 tumor homogenate. n=6. (H) Representative immunohistochemistry staining with anti-CD68 antibodies of MC38 tumor samples collected from the vehicle or VBL (1.25 mg/kg weight, every other day for 2 w) treatment. (I–J) Perimeter (I) and circularity (J) of CD68-positive cells in panel (H) were counted. (K) Workflow for VBL treatment with or without T cells (anti-CD8) or macrophage (anti-CSF1R) depletion; s.c., subcutaneously; i.p., intraperitoneally. (L) Growth curve of MC38 tumors during VBL treatment with or without immune cell depletion. n=6. (M) Tumor weight at the end of treatment in panel (L). n=6. (N–O) Flow cytometry analysis for total macrophages (N) and T cells (O) in MC38 tumors after VBL treatment with or without immune cell depletion. n=6. Data are presented as mean \pm SD. Data in (A, L) were analyzed using a two-way ANOVA with time and treatment type as covariates. *Represents VBL+IgG versus Vehicle+IgG; ##represents VBL+ anti-CSF1R versus VBL+IgG; ††represents VBL+anti-CD8 versus VBL+IgG. Data in (B–K, N–P) were analyzed using a two-tailed Student's t-test for comparisons. P values were determined by a two-tailed Student's t-test. *p<0.05, **p<0.01, ***p<0.001. ANOVA, analysis of variance; TAM, tumor-associated macrophage; VBL, vinblastine.

M1-like macrophages were reported to promote CD8⁺ T cell activation by secreting IL-12 or IFN γ . Our previous results also indicated that VBL-treated macrophages may recover CD8⁺ T cell proliferation by secreting certain cytokines, so ELISA was performed to detect the secretion of IFN- γ and IL-12 in tumor tissues. The results demonstrated that the protein levels of IL-12 and IFN γ were significantly increased in both tumor models after VBL administration (figure 2F,G, online supplemental figure 2E,F). In line with the above finding, the IL-12 and IFN γ levels in CM collected from BMDM-derived TAMs were also significantly increased following VBL treatment (online supplemental figure 2G,H). Intriguingly, although we found that VBL attenuated differentiation of monocytes to macrophages in tumors (figure 2B, online supplemental figure 2B), VBL has no effect on the differentiation of monocyte into macrophages in vitro (online supplemental figure 2I), suggesting that the more complex microenvironment in vivo may lead to differences in the functions of VBL when compared with in vitro at least to some extent.

Meanwhile, the cytokines IL-12 and IFN γ secreted from CD8⁺ T cells remained unchanged both in vitro (online supplemental figure 2J,K) and in vivo (online supplemental figure 2L,M) after direct VBL treatment. These findings indicate that VBL-treated macrophages could secrete IL-12 and IFN γ to promote CD8⁺ T cell activation, although we could not rule out the contribution of other cells in releasing these cytokines. Histology staining of the macrophage marker CD68 showed that macrophages in tumors exhibited an M1-like round and flattened morphology after VBL treatment, which was verified by the reduced cell perimeter and increased cell circularity. In contrast, the elongated M2-like macrophages

were more prevalent in vehicle-treated tumor samples (figure 2H-J).

Furthermore, in vivo antibody depletion experiments were performed to test whether macrophages and CD8⁺ T cell populations were required for the antitumor effect of VBL (figure 2K). Macrophage and CD8⁺ T cell depletion both reduced the antitumor efficacy of VBL in MC38 colorectal tumors, suggesting that both macrophages and CD8⁺ T cells are indispensable in VBL immunotherapy (figure 2L,M). Moreover, cell depletion efficiency was confirmed by flow cytometry (figure 2N,O). Collectively, these results reveal that VBL can control tumor growth and re-educate M2-like TAMs into antitumor M1-like phenotype in vivo, and the prominent tumor suppression function requires both macrophages and CD8⁺ T cells.

VBL combined with PD-1 blockade enhances immunotherapy

Considering the limitations of anti-PD-1 in inhibiting colorectal tumors, the efficiency of VBL and anti-PD-1 combination therapy was investigated in comparison with monotherapy. MC38 tumor models were established and VBL was coadministered with anti-PD-1 (figure 3A). After combination therapy, tumor development was almost completely suppressed (figure 3B,C). Although VBL treatment decreased macrophage infiltration in tumors, anti-PD-1 treatment alone appeared to increase the proportion of macrophages in tumors (figure 3D). The combined VBL and anti-PD-1 treatment resulted in an increased M1/M2 ratio, but was not significantly higher than monotherapy (figure 3E). VBL and anti-PD-1 combination maximized the proportion of CD8⁺ T cells in the tumor compared with monotherapy (figure 3F), indicating an enhanced immunotherapy effect. Overall, these results indicated that the combination of VBL and

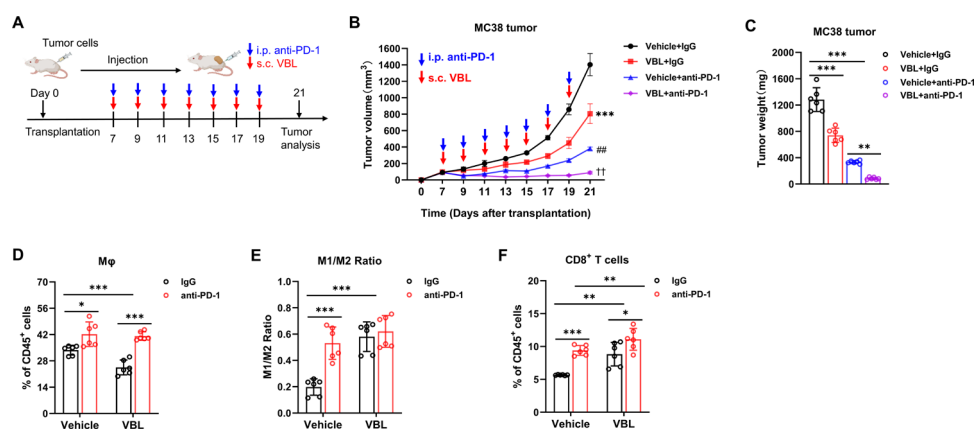


Figure 3 VBL combined with PD-1 blockade enhances immunotherapy. (A) Schematic experimental workflow for combination treatment; s.c., subcutaneously; i.p., intraperitoneally. (B) Growth curve of MC38 tumors under anti-PD-1 treatment combined with VBL treatment. n=6. (C) Tumor weight at the end of treatment in panel (A). (D-F) Flow cytometry analysis for percentage of total macrophages (D), M1/M2 ratio (E), and percentage of T cells (F) in MC38 tumors after anti-PD-1 treatment combined with VBL treatment. n=6. Data are presented as mean±SD. Data in (B) were analyzed using a two-way ANOVA with time and treatment type as covariates. *Represents VBL+IgG versus vehicle+IgG; ##represents Vehicle+anti-PD-1 versus VBL+IgG; ††represents VBL+anti-PD-1 versus vehicle+anti-PD-1. Data in (C-F) are analyzed using a two-tailed Student's t-test for comparisons. P values were determined by a two-tailed Student's t-test. *p<0.05, **p<0.01, ***p<0.001. ANOVA, analysis of variance; VBL, vinblastine.

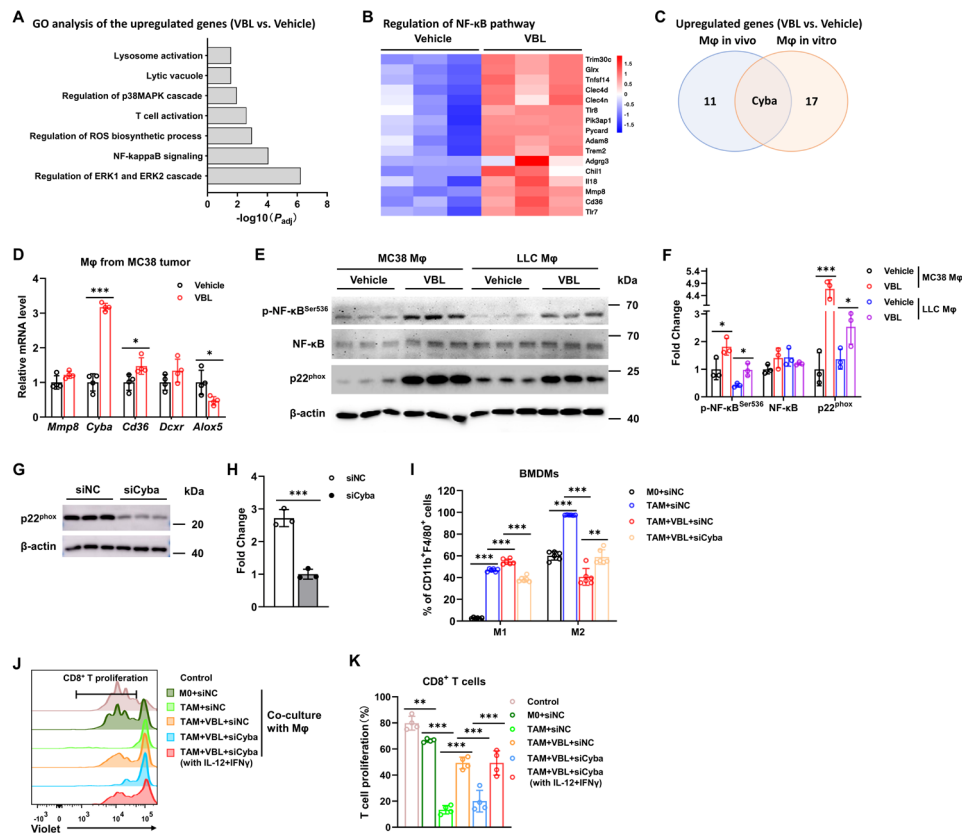


Figure 4 VBL targets NF- κ B-Cyba to reprogram macrophages. (A) Gene ontology analysis of RNA-sequencing data collected from BMDMs with or without VBL treatment for 24 hours. (B) A heatmap of genes related to the NF κ B pathway from RNA-sequencing data collected from macrophages (M ϕ in vivo), sorted and analyzed from Vehicle/VBL treated tumors. The heatmap was created based on the normalized FPKM of genes in the NF- κ B pathway. (C) Venn diagrams of upregulated genes enriched in ROS production pathway. (D) Gene expression of *Mmp8*, *Cyba*, *Cd36*, *Dcxr*, and *Alox5* in macrophages sorted from MC38 tumors. $n=4$. (E) Representative western blot against p-NF- κ B, NF- κ B, p22^{phox}, and β -actin in macrophages sorted from indicated tumor samples. (F) Fold change of p-NF- κ B, NF- κ B, and p22^{phox} protein level in panel (E). $n=3$. (G) Representative western blot against p22^{phox} and β -actin in BMDMs. (H) Fold change of p22^{phox} protein levels in panel (G). $n=3$. (I) Flow cytometry analysis for percentages of M1 (F4/80⁺CD11b⁺CD86⁺) and M2 (F4/80⁺CD11b⁺CD206⁺) BMDMs after the corresponding treatment for 24 hours. $n=6$. (J) Representative flow cytometry results of T cell proliferation after co-culture with BMDMs for 72 hours. (K) Statistical results of T cell proliferation in panel (J). $n=6$. Data are presented as mean \pm SD. P values were determined by a two-tailed Student's t-test. * $p<0.05$, ** $p<0.01$, *** $p<0.001$. BMDMs, bone marrow-derived macrophages; ROS, reactive oxygen species; VBL, vinblastine.

anti-PD-1 could enhance the immunotherapy efficiency and almost completely inhibit tumor growth.

VBL targets NF- κ B-Cyba to reprogram macrophages

Next, the molecular mechanism through which VBL resets TAMs was explored. Bulk RNA sequencing (RNA-seq) was first performed to explore the changes in gene expression profiles. Macrophages differentiated from BMDMs (in vitro M ϕ) and sorted from MC38 colorectal tumor (in vivo M ϕ) with or without VBL treatment were collected separately for RNA-seq. Gene ontology (GO) analysis was performed, which revealed an enhanced nuclear factor kappa-B (NF- κ B) signaling pathway, a transcription factor that plays a key role in immune responses, both in macrophages in vitro and in vivo (figure 4A,B). RNA-seq of the two macrophage datasets also revealed that regulation of ROS biosynthetic pathway was activated, among which *Cyba* (encodes the p22^{phox} nicotinamide adenine

dinucleotide phosphate (NADPH) oxidase subunit) was the only upregulated gene in both datasets (figure 4A,C; online supplemental figure 3A). Several genes from the RNA-seq results were selected for verification, and *Cyba* was very likely to be one of the target genes (figure 4D, online supplemental figure 3B), of which the expression could also be regulated by NF- κ B.^{23 24}

Activated phosphorylated NF- κ B and p22^{phox} protein levels were both significantly elevated in macrophages sorted from colorectal MC38 tumors or LLC pulmonary tumors (figure 4E,F). Furthermore, phosphorylated NF- κ B and p22^{phox} were also upregulated in VBL-treated BMDMs (online supplemental figure 3C,D). *Cyba* was knocked down in macrophages by siRNA interference (figure 4G,H), and the VBL-induced increase of M1 polarization and decrease of M2 polarization were both significantly abrogated (figure 4I), as well as

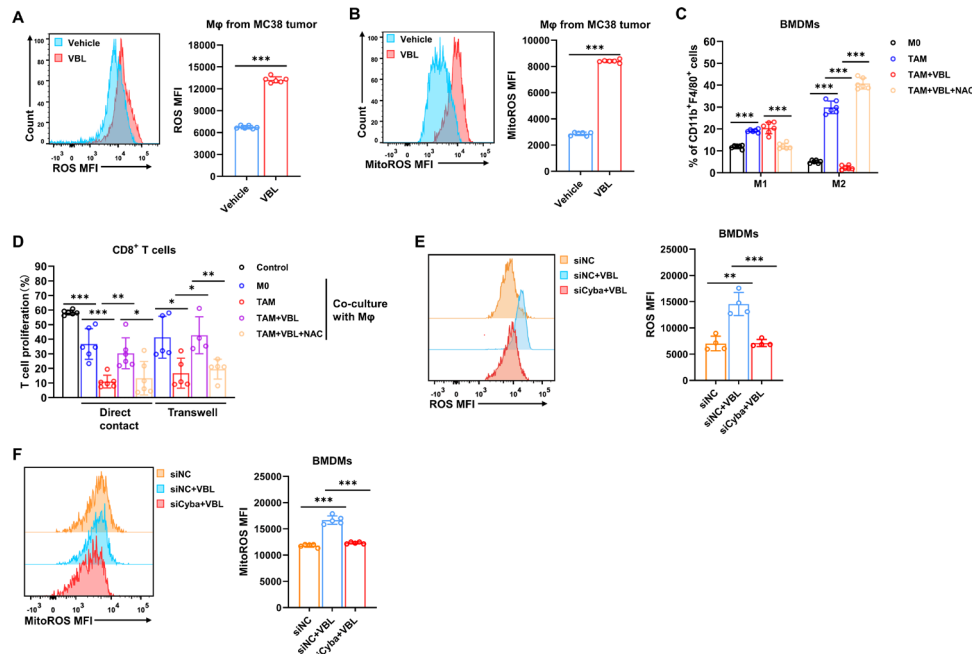


Figure 5 VBL-induced ROS repolarizes TAMs. (A, B) Flow cytometry analysis of cytosolic ROS (A) and mitoROS (B) levels in macrophages sorted from Vehicle/VBL treated MC38 tumors. $n=6$. (C) Flow cytometry analysis for percentages of M1 (F4/80⁺CD11b⁺CD86⁺) and M2 (F4/80⁺CD11b⁺CD206⁺) in BMDMs under the corresponding treatment for 24 hours. $n=6$. (D) T cell proliferation ratio after co-culture with macrophages by direct contact or transwell. $n=4-5$. (E, F) Flow cytometry analysis of cytosolic ROS (E, $n=4$) and mitoROS (F, $n=5$) levels in BMDMs with or without Cyba knockdown. Data are presented as mean \pm SD. P values were determined by a two-tailed Student's t-test. * $p<0.05$, ** $p<0.01$, *** $p<0.001$. BMDMs, bone marrow-derived macrophages; MFI, mean fluorescence intensity; ROS, reactive oxygen species; VBL, vinblastine.

the CD86 and CD206 expression levels (online supplemental figure 3E). Macrophages treated with VBL after Cyba knockdown lost their ability to activate CD8⁺ T cells (figure 4J,K). However, addition of recombinant IL-12+IFN γ significantly rescue CD8⁺ T cell proliferation in context of co-culture with Cyba-depleted macrophages, suggesting that VBL induces these cytokines secretion in macrophages and thus promoting CD8⁺ T cell activation (figure 4J,K). GO analysis also demonstrated that proinflammatory cytokines IL-12, TNF, IFN γ , IL-1 β , and IL-6 were all increased after VBL treatment (online supplemental figure 3F-H). In addition, GSEA analysis revealed that NF- κ B signaling, TNF signaling, and T cells mediated cytotoxicity pathways were enriched in VBL-treated macrophages (online supplemental figure 3I-K). Collectively, these results suggested that VBL-stimulated macrophages were repolarized to the M1-like phenotype via the NF- κ B-Cyba signaling pathway.

VBL-induced ROS repolarizes TAMs

Since p22^{phox} is an important component of the superoxide-generating NADPH oxidases (NOXs), p22^{phox}-NOX complexes are one of the most critical sources of ROS in cells and tissues.^{25,26} Subsequently, the ROS levels in macrophages after VBL treatment were evaluated. Both cytosolic ROS and mitochondrial ROS (mitoROS) were elevated in macrophages sorted from VBL-treated MC38 tumors and LLC tumors (figure 5A,B, online supplemental figure 4A,B), as well as BMDMs after VBL treatment (online supplemental figure 4C,D).

ROS was depleted by using the ROS scavenging reagent N-acetylcysteine (NAC), resulting in significant abrogation of VBL-induced M1 polarization and restored M2 polarization (figure 5C). Consistent with this phenotype, macrophages treated with VBL during ROS depletion dramatically lost their ability to recover CD8⁺ T cell proliferation in both direct contact and transwell co-cultures (figure 5D). As expected, Cyba knockdown by siRNA interference significantly hindered ROS and mitoROS production from VBL-treated macrophages (figure 5E,F). In conclusion, these results indicated that the NF- κ B-Cyba-ROS axis is a crucial signaling pathway in VBL-induced TAM repolarization.

ROS-activated transcription factor EB promotes lysosome activation and biogenesis

Recent research showed that ROS induces autophagy and lysosome biogenesis by regulating nuclear transcription factor EB (TFEB) nuclear translocation.²⁷⁻²⁹ The RNA-seq data also showed significant upregulation in the lysosome activation pathway (figure 4A and figure 6A). Moreover, immunofluorescence staining of lysotracker revealed that VBL treatment induced a marked lysosome increase in macrophages (figure 6B,C). Flow cytometry analysis of lysosome membrane protein Lamp1 expression also indicated elevated lysosome contents (figure 6D,E). Although colchicine and paclitaxel could increase the content of lysosomes in macrophages compared with the control group, far fewer lysosomes were present compared with the VBL-treated group (online supplemental figure 5A,B).

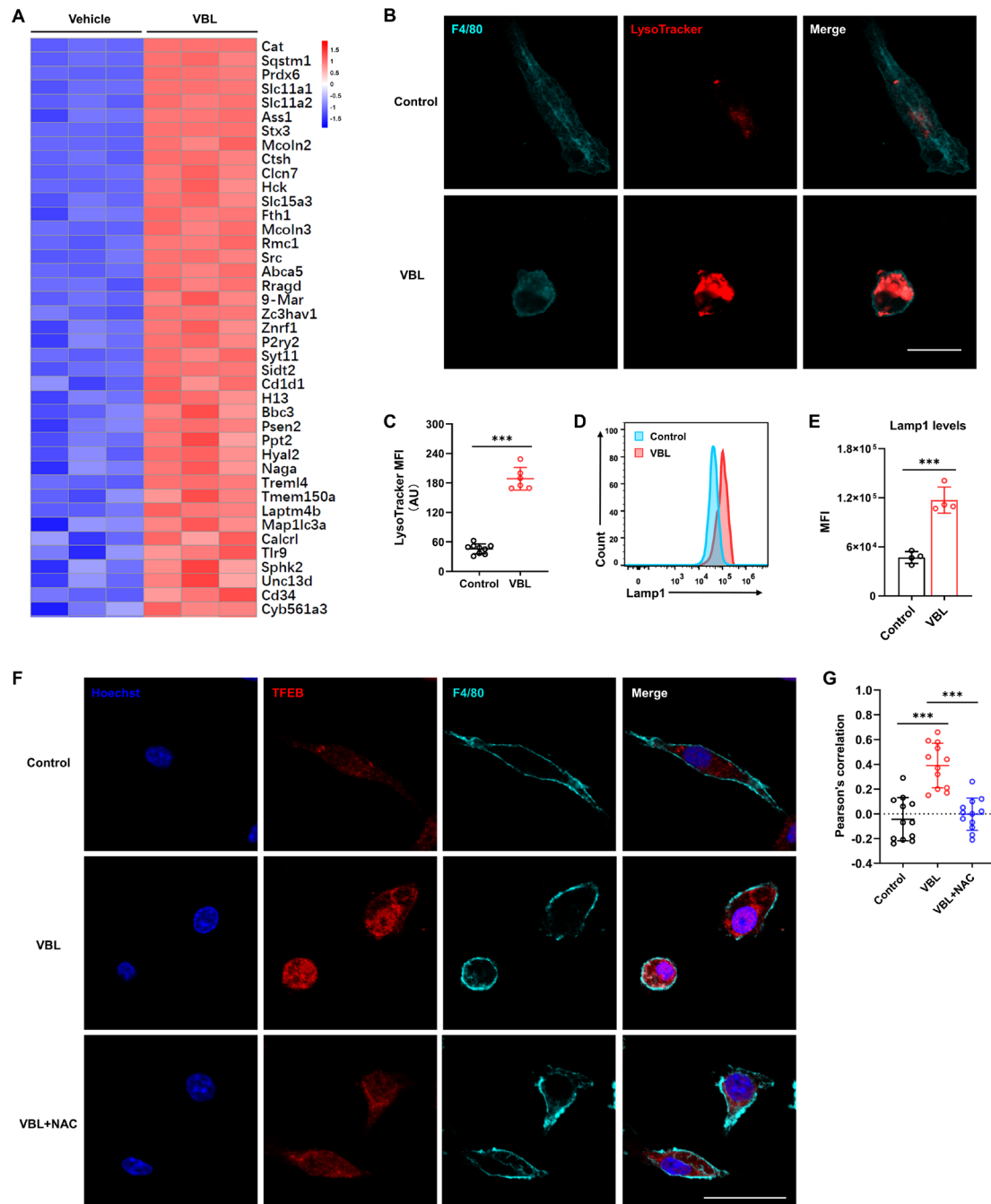


Figure 6 ROS-activated TFEB promotes lysosome activation and biogenesis. (A) RNA-sequencing data was collected from BMDMs (Mφ in vitro) with or without VBL treatment for 24 hours, and the heat map was created based on normalized FPKM of genes in the lysosome pathway. (B) Immunostaining with F4/80 and LysoTracker showed the changes in lysosome levels in BMDMs after VBL treatment. (C) Statistical results of LysoTracker MFI in panel (B). n=9 (control). n=6 (VBL). (D) Representative flow cytometry results of Lamp1 in BMDMs after VBL treatment for 24 hours. (E) Statistical results of Lamp1 MFI in panel (D). n=4. (F) Immunostaining with TFEB, F4/80, and Hoechst in BMDMs after indicated treatment for 24 hours. (G) Statistical results of TFEB and Hoechst colocalization in (F). n=12. Data are presented as mean±SD. P values were determined by a two-tailed Student's t-test. *p<0.05, **p<0.01, ***p<0.001. BMDMs, bone marrow-derived macrophages; MFI, mean fluorescence intensity; VBL, vinblastine.

Meanwhile, significantly higher levels of TFEB nuclear translocation were observed in VBL treated macrophages compared with the control group, which was significantly inhibited after ROS clearance by NAC (figure 6F,G).

These findings demonstrated that VBL-induced TFEB nuclear translocation was dependent on ROS production.

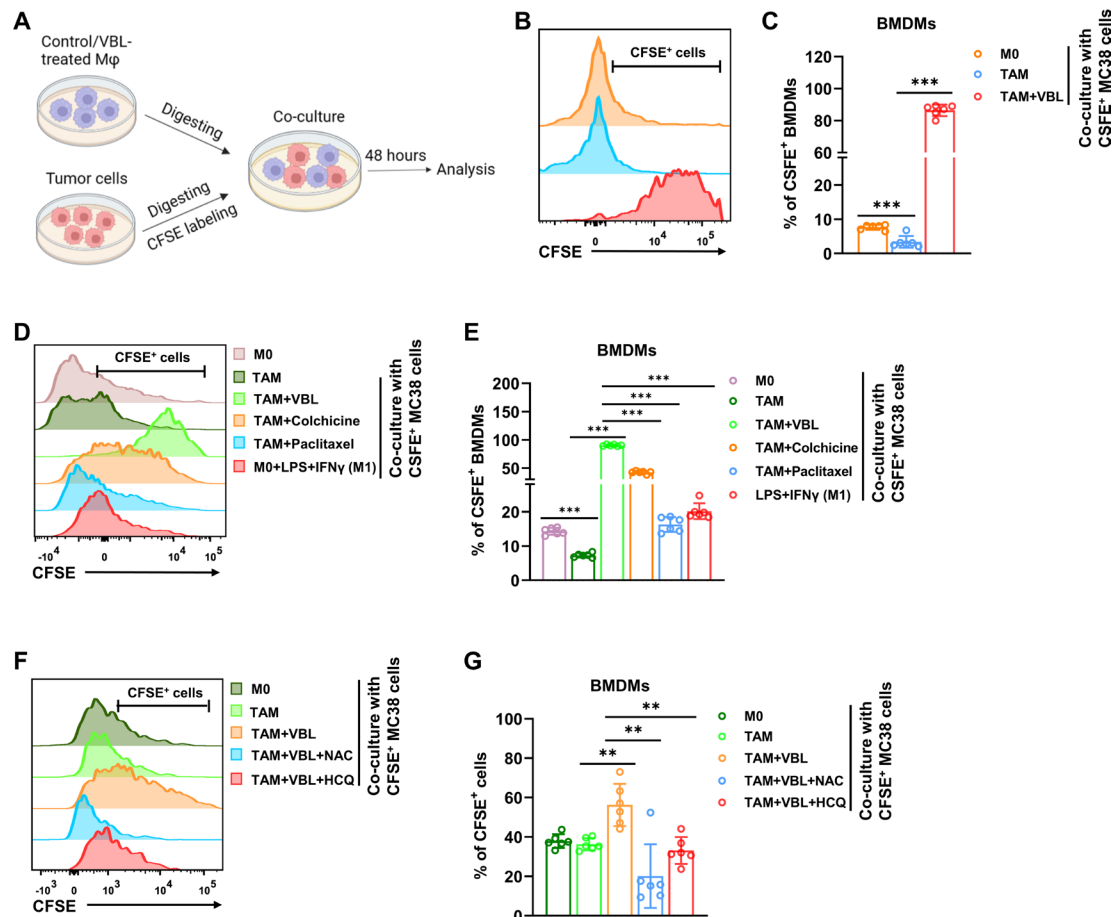


Figure 7 VBL reprograms macrophages to be tumoricidal through increased phagocytic capacity. (A) Schematic experimental workflow for evaluating the phagocytic capacity of macrophages. (B) Representative flow cytometry results of BMDMs after VBL treatment and co-culture with CFSE⁺ MC38 tumor cells. (C) Statistical results of CFSE⁺ BMDMs in (B). n=6. (D) Representative flow cytometry results of BMDMs after different treatments and co-culture with CFSE⁺ MC38 tumor cells. (E) Statistical results of CFSE⁺ BMDMs in (D). n=6. (F) Representative flow cytometry results of VBL-induced BMDMs after ROS scavenging (NAC) or lysosome inhibition (HCQ) and co-culture with CFSE⁺ MC38 tumor cells. (G) Statistical results of CFSE⁺ BMDMs in (F). n=6. Data are presented as mean±SD. P values were determined by a two-tailed Student's t-test. **p<0.01, ***p<0.001. BMDMs, bone marrow-derived macrophages; CFSE, carboxyfluorescein succinimidyl amino ester; HCQ, hydroxychloroquine; NAC, N-acetylcysteamine; ROS, reactive oxygen species; VBL, vinblastine.

VBL reprograms macrophages to be tumoricidal through increased phagocytic capacity

Defective lysosomal degradation has been linked to attenuated phagocytosis.³⁰ However, whether increased lysosomal activity enhances phagocytic capacity has not been reported. The effect of VBL treatment on the phagocytic capacity of macrophages was explored (figure 7A). Both BMDMs and TAMs showed low tumor cell phagocytic capacity, whereas VBL-treated macrophages displayed dramatically increased MC38 (figure 7B,C) and LLC tumor cell phagocytosis (online supplemental figure 6A). In accordance with their lysosomal activity, colchicine and paclitaxel treatment only marginally increased phagocytosis of both tumor cells (figure 7D,E, online supplemental figure 6B,C). This increased phagocytosis was not due to increased apoptosis of tumor cells, as CM from VBL-treated macrophages only slightly increased the proportion of Annexin V⁺ tumor cells (online supplemental figure 6D). Notably, the classically activated (LPS+IFNγ induced) M1 macrophages

did not show a significant increase in phagocytic capacity (figure 7D,E, online supplemental figure 6B,C), suggesting the unique role of VBL in inducing phagocytosis.

Subsequently, the roles of ROS and lysosomes in VBL-induced phagocytosis enhancement were explored by using the ROS scavenging reagents NAC and lysosome inhibitor hydroxychloroquine (HCQ). Either NAC or HCQ treatment could dramatically abolish the increased phagocytic capacity induced by VBL (figure 7F,G), suggesting that ROS and lysosome activation play a critical role in VBL-induced phagocytosis in macrophages. Collectively, these results suggested for the first time a direct link between increased lysosomal activity to sustained phagocytic capacity, which can be enhanced in TAMs on VBL treatment.

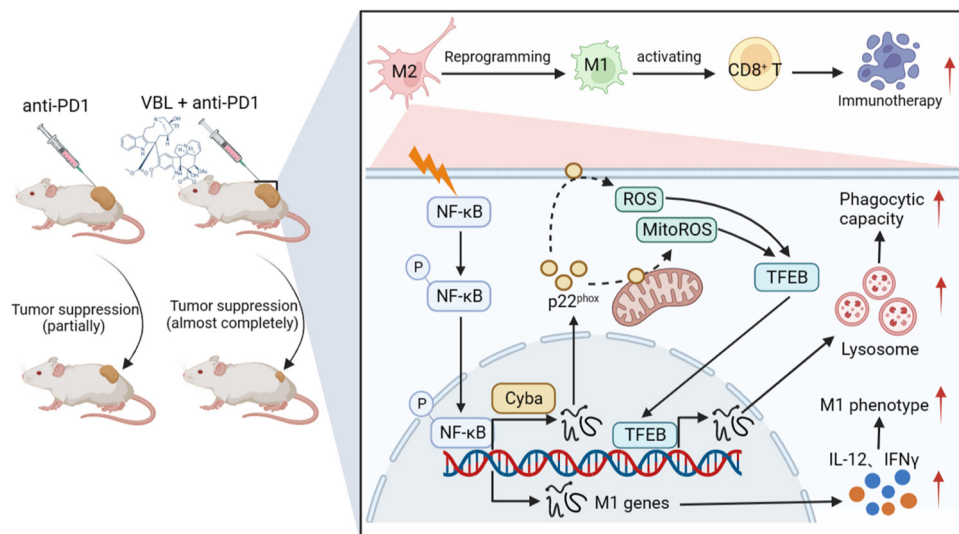


Figure 8 Working model for VBL-mediated antitumor immune response. VBL phosphorylates and activates the transcription factor NF- κ B in TAMs, upregulating cyba which encodes p22^{phox} protein expression. Cytosolic ROS and MitoROS levels were increased by p22^{phox}-catalyzed synthesis. ROS further facilitated the entry of transcription factor TFEB into the nucleus, accelerating lysosome biogenesis and activation, and thus endowing TAMs with a higher phagocytic capacity. ROS also repolarized TAMs into the M1-like phenotype and abolished their suppressive activity on CD8⁺ T cells. This graph model was created with biorender.com. ROS, reactive oxygen species; TAMs, tumor-associated macrophage; VBL, vinblastine.

DISCUSSION

The antitumor effects of VBL have long been attributed to the inhibition of tumor cell division by targeting microtubule depolymerization, but the immunomodulatory effect of VBL has been ignored for a long time. Our study provides new evidence that the antitumor effect of VBL in promoting immune response in tumors by reprogramming M2-like TAMs into M1-like antineoplastic phenotype and subsequently activating CD8⁺ T cells, at least in part, through the NF- κ B-Cyba-ROS axis (figure 8).

Microtubules are highly dynamic cytoskeletal fibers composed of α -tubulin and β -tubulin heterodimers, which are the cellular targets of many chemotherapy drugs that either stabilize or destabilize microtubules.^{31 32} Dynamic microtubules have become one of the most successful cancer chemotherapeutic targets, such as paclitaxel targeting microtubule depolymerization, which is among the most effective microtubule-targeted chemotherapeutic drugs.³¹ Similar to VBL, paclitaxel treatment also repolarized TAMs into M1-like phenotype based on surface marker expression. However, paclitaxel neither reversed the immunosuppressive effect nor increased the phagocytic capacity of TAMs (figure 1E,F; figure 7D,E), indicating a specific function of VBL in activating antitumor immunity. Microtubule-targeting agents (MTAs) can be largely divided into MT-stabilizing agents (such as paclitaxel) and MT-destabilizing agents (such as colchicine and VBL). Different MTAs have different binding sites on the tubulin dimers, which might account for the different effects of the MTAs used in this study on modulating macrophages. Natoli *et al* reported that plinabulin, an MTA sharing the same binding site as colchicine, induced M1 polarization via the JNK signaling pathway.³³ In addition, treatment

with colchicine induced M1 macrophage polarization, as defined by surface marker expression. However, similar to paclitaxel, colchicine treatment did not reverse the suppressive function of TAMs. Nevertheless, these studies suggested that despite the common mechanism of interrupting MT dynamics, different MTAs exert vastly different functions in modulating immune cells. As many of these drugs have been used for centuries to treat inflammatory diseases and cancer, further studies of the detailed molecular pathways underlying the mechanisms of action of these drugs on different cells will increase the effectiveness of MTAs.

Chemotherapy and immunotherapy are the most effective antitumor therapies in clinical practice besides surgical resection. Several studies have reported roles of macrophages in amplifying cytotoxic effects of chemotherapy.^{34 35} But paradoxically, other studies demonstrated that TAMs limit chemotherapy induced mitotic arrest, resulting in continued cancer cell proliferation. Previous studies suggested high dose taxol promoted TAM infiltration in breast tumor through a cathepsin dependent manner, thereby inhibiting tumor cell death.^{36 37} However, in our study, continuous low-dose VBL injection can reduce TAM infiltration in mouse tumors. Therefore, in addition to the pleiotropic effect on tumor cells, more and more evidences show that some chemotherapy drugs have changed the tumor microenvironment, as we describe here for VBL in colon cancer. Clearly, the effect of these chemotherapy drugs depends on the types of tumor and immune cell phenotypes in tumor microenvironment. Further studies of the mechanism of action of VBL in other types of tumor may provide opportunities to develop a more effective cancer immunomodulatory strategy.

Our research shows that VBL can not only activate T cells by changing the phenotype of macrophages, but also activate the lysosome of macrophages and thus endowing them stronger phagocytotic ability. Studies have shown that in the process of tumor development, lysosome of tumor cells increases in size and activity to meet the rapid growth and metabolic needs of tumor cells. The highly active lysosome in tumor cells can uptake and store some chemotherapy drugs, thus decreasing treatment efficacy. Therefore, there are some specific targeted drugs developed for tumor lysosome.^{38,39} However, the treatment efficacy of VBL is rather abolished in the absence of macrophages in our model, therefore, it is unlikely that VBL is trapped in lysosome in macrophages.

The results suggested that VBL treatment transcriptionally upregulated *Cyba* expression, resulting in increased ROS generation, which further repolarized TAMs to the M1-like phenotype. ROS scavenger NAC treatment or siRNA-mediated *Cyba* knockdown abolished the repolarization effect of VBL on TAMs. However, the role of ROS in inducing macrophage polarization remains controversial. ROS are involved in both pro-inflammatory and anti-inflammatory control of macrophage polarization. Research reported that ROS plays an essential role in the activation of p38 MAPK and NF- κ B signaling pathways, subsequently promoting pro-inflammatory gene expression in macrophages.^{40–42} However, other studies have shown that inhibition of ROS production in human monocytes prevents M2-like polarization and the subsequent response to M2-polarizing cytokine IL-4.^{41,43,44} Overall, the conditions for preferential activation of M1- or M2-like polarization remain unclear. The present study demonstrates that VBL repolarizes macrophages to the M1-like phenotype via the NF- κ B-*Cyba*-ROS axis and activates CD8⁺ T cells to suppress tumor growth, consequently promoting antitumor immune response.

Antitumor therapies involving the use of immune-checkpoint inhibitors such as anti-PD-1 have emerged as new therapeutic pillars within oncology. These antibodies target regulatory pathways in T cells to enhance anti-tumor immune responses, which has led to major clinical advances and provided a new strategy against cancer. However, for colorectal cancers and other tumors, the effect of T-cell checkpoint-blocking therapy is limited. Furthermore, combined immunotherapy for CD8⁺ T cell activation is currently under-research. The current study demonstrates that VBL reprograms macrophages to the M1-like phenotype via the NF- κ B-*Cyba*-ROS axis and then activates CD8⁺ T cells to inhibit tumor growth, thus enhancing immunotherapy when combined with an anti-PD-1 monoclonal antibody. These findings highlight the potential of a new combination therapeutic strategy to treat malignant tumors.

MATERIALS AND METHODS

Animals

All mice were congenic to the C57BL/6/J background and were purchased from SLAC Biotechnology. Mice were housed under a 12-hour light-dark cycle in plastic cages and fed an irradiated chow diet. Housing temperatures and humidity were kept within 21.7°C–22.8°C and 40%–60%, respectively. The water and cages were autoclaved. Cages were changed once weekly, and the health status of the mice was monitored using a dirty bedding sentinel program. The mice were allowed free access to food and water. Unless otherwise indicated, male mice at 7–8 weeks of age were used in these studies. For all in vivo studies, cohorts of greater than or equal to three mice per treatment were assembled, and experiments were independently repeated two to three times.

Tumor mouse models

The MC38 colorectal tumor cell line and LLC pulmonary tumor cell line were purchased from American Type Culture Collection. The tumor cells (1×10^6 cells/mouse in 100 μ L PBS) were subcutaneously injected into the posterior back or armpit area of the C57BL/6/J mice to establish the transplanted tumor models.

Cell culture

The MC38 and LLC tumor cells were cultured in Dulbecco's modified Eagle's medium (DMEM) (Gibco) supplemented with 10% (v/v) fetal bovine serum (FBS) (Sigma-Aldrich). During the culture period, the medium containing new FBS was replaced every other day. All cells were cultured and maintained at 37°C in a 5% CO₂ incubator, and the medium was supplemented with 1% penicillin and 1% streptomycin (Invitrogen).

Culture of BMDM

Bone marrow cells were isolated from the femur and tibia of 6–7 weeks male C57BL/6J WT mice and differentiated to mature macrophages for 7 days as described previously.⁴⁵ Briefly, cells were maintained in DMEM with 10% FBS, containing 10 ng/mL M-CSF (PeproTech). On day 7, a CM collected from tumor cells was added for TAM differentiation for 24 hours.

BMDMs and tumor cell co-culture assay

BMDMs were first planted on a 12-well plate and treated with different reagents after differentiation. The tumor cells were collected and labeled with carboxyfluorescein succinimidyl amino ester (CFSE, 1 μ M, Invitrogen) fluorescence dye. After macrophages pretreated with VBL before co-culturing with tumor cells, reagents were removed from BMDMs culture medium. Then tumor cells were added to the BMDMs culture plate in proportion for 48 hours of co-culture.

CD8⁺ T cells activation assay

CD8⁺ T cells were isolated from the spleens of 6–7 weeks male C57BL/6J WT mice with a CD8⁺ magnetic cell sorting Kit (Miltenyi Biotec, 130-117-044) according

to the manufacturer's instructions. Macrophages were differentiated from the bone marrow of these mice and were pretreated with VBL before co-culturing with T cells. VBL was washed out from BMDMs culture medium with PBS. Both macrophages and T cells were placed into the plate, which was coated with CD3 (Biolegend, 100340) according to a certain proportion for co-culture. CD8⁺ T cells were labeled with fluorescent Violet dye and then cultured with or without macrophages under different experimental conditions for 72 hours, in RPMI-1640 medium with 20% FBS, 200 mM L-glutamine, 100 mM sodium pyruvate, 50 mM 2-mercaptoethanol, and supplied with purified anti-mouse CD28 antibody (Biolegend, 102101) costimulatory factor. To isolate and purify CD8⁺ T cells in MC38 tumor, tumors were mechanically minced and digested with 0.075% collagenase I (Sigma-Aldrich) and 0.075% collagenase III (Sigma-Aldrich) in PBS containing DNase I (4U/mL) at 37°C for 45 min to 1 hour. Subsequently, the cells were lysed with ACK lysis buffer and filtered with a 40 µm cell strainer. CD8⁺ T cells were isolated from tumors with a CD8⁺ magnetic cell sorting Kit (Miltenyi Biotec, 130-117-044) according to the manufacturer's instructions and then treated with VBL for 24 hours. The violet or mean fluorescence intensity (MFI) was detected as an activation indicator of CD8⁺ T cells by flow cytometry.

NK cells isolation and analysis

The spleen single cell suspension were lysed with ACK lysis buffer and then selected using a EasySep Mouse NK magnetic cell sorting Kit (STEMCELL Technologies, 19855) according to manufacturer's instruction. The NK1.1⁺ NK cells were treated with VBL for 24 hours and then CD69 MFI was analyzed by flow cytometry.

CM transfer assay

In the CM transfer assay, the original tumor cell culture medium was discarded and the cells were gently washed with fresh blank medium. Then, fresh medium without any additional agents was added and the cells were cultured for another 24 hours. Finally, the medium was collected as CM.

In vivo tumor experiments

In vivo, tumor size was measured with calipers, and tumor volume was calculated by the formula $\text{volume} = (\text{length} \times \text{width}^2) / 2$. Treatment was initiated when tumors reached 5–6 mm in size (approximately the 7th day) and 1.25 mg/kg weight VBL (Selleck) was injected into the tumors subcutaneously according to the indicated frequency. The total volumes of all tumors were calculated for each mouse and reported.

For the anti-PD1 combination therapy experiments, 100 µg/mouse anti-PD1 (BioXCell, BE0146) monoclonal antibodies were injected into tumor-bearing mice through intraperitoneal injection, and 1.25 mg/kg weight VBL were injected subcutaneously around the tumors according to the indicated frequency.

For the immune cell depletion experiments, anti-CD8 (BioXCell, BE0004-1) or anti-CSF1R (BioXCell, BE0213) antibodies were injected intraperitoneally 1 day before treatment with VBL. For the depletions, 0.2 mg of anti-CD8 or 0.5 mg of anti-CSF1R were injected per mouse according to the indicated frequency.

Flow cytometry

Two days after the last intraperitoneal or subcutaneous injection, tumors were mechanically minced and digested with 0.075% collagenase I (Sigma-Aldrich) and 0.075% collagenase III (Sigma-Aldrich) in PBS containing DNase I (4U/mL) at 37°C for 45 min to 1 hour. Subsequently, the cells were lysed with ACK lysis buffer and filtered with a 40 µm cell strainer. For flow cytometry staining, cells (1×10^6) were incubated with mouse Fc receptor blocker (Biolegend) at 4°C for 20 min, then stained with the appropriate antibodies to surface markers at 4°C for 20 min in the dark, and/or fixed/permeabilized (Fixation/Permeabilization Solution Kit, Biolegend) and stained with intracellular antibodies at 4°C for 30 min. The stained single cells were analyzed using a Fortessa flow cytometer (BD Biosciences). The data were analyzed with FlowJo V.10.7.0 (BD Biosciences). Gates were constructed to identify target populations based on surface marker staining. Mainly, M2-like TAMs were identified as CD45⁺CD11b⁺F4/80⁺CD206⁺, and M1-like macrophages were identified as CD45⁺CD11b⁺F4/80⁺CD86⁺.

The following commercial antibodies were used: CD45-PE/Cyanine7 (Biolegend, 103114), CD45-PerCP/Cyanine5.5 (Biolegend, 103132), CD11b-APC/Cyanine7 (Biolegend, 101226), F4/80-PE (Biolegend, 123110), CD206-APC (Biolegend, 141708), CD86-FITC (Biolegend, 105005), CD8α-APC (Biolegend, 100712), CD8α-FITC (Biolegend, 100705), CD69-FITC (Biolegend, 104505), NK1.1-APC (Biolegend, 156506). All the antibodies were used at a 1: 500 dilution in 1% FBS in PBS.

RNA extraction and quantitative real-time PCR

RNA was extracted from cultured cells using TRIzol (Invitrogen). Normalized RNA was reversed transcribed using RevertAid First Strand cDNA Synthesis kit (Thermo Fisher) and cDNA was analyzed by qRT-PCR with the 7500 Fast Real-Time PCR System (Applied Biosystems). Subsequently, relative mRNA levels were calculated using the comparative CT method and normalized to 18S rRNA mRNA. The average of the control group was set as one, and all the results were presented as the relative mRNA expression. All primers used are listed with their sequences in online supplemental table 1.

Western blot

For western blotting, whole cell lysates were lysed in 2% sodium dodecyl sulfate (SDS) buffer containing protease inhibitor cocktail (Roche) and phosphatase inhibitor cocktail (Roche). A protein of 10–30 µg was separated by SDS-PAGE and then transferred onto a polyvinylidene fluoride (0.22 µm) transfer membrane using the wet

transfer method. Membranes were blocked with 5% fat-free milk in TBST (Tris-buffered saline plus 0.1% Tween-20) for 1 hour at room temperature, and the membranes were incubated in primary antibodies overnight at 4 °C. The next day, the membranes were washed in TBST (3×10 min) and then incubated with HRP-conjugated secondary antibodies for 1 hour at room temperature. After TBST washes (4×10 min), Pierce ECL western blotting substrate was added onto the membrane and incubated for 2 min to develop the chemiluminescent signal.

The following commercial antibodies were used: anti-phospho-NF-κB (Cell Signaling Technology, 3033S), anti-NF-κB (Cell Signaling Technology, 8242S), anti-p22^{phox} (Cell Signaling Technology, 27297S), anti-β-actin (Sigma A1978), anti-mouse (Abcam ab6728), anti-Rabbit (Abcam ab6721). All the primary antibodies were used at a 1:1000 dilution in 3% bovine serum albumin (BSA) in TBST. Secondary antibodies were used at a 1:5000 dilution in 5% non-fat milk in TBST.

Histology

Freshly isolated tumor tissue was fixed in 4% paraformaldehyde for 24 hours at room temperature. Tissues were embedded in paraffin, sectioned at 8 μm thickness, deparaffinized, and rehydrated through graded concentrations of ethanol in water. Sections were then probed with primary antibodies against CD68 (Abcam ab283654, 1:500), followed by biotinylated secondary antibodies. The binding of the secondary antibodies was visualized by using diaminobenzidine chromogen A (Thermo Fisher).

Immunofluorescence imaging

BMDMs were fixed with 2% PFA, permeabilized with a buffer containing 0.1% Triton X-100 and 0.25% BSA, and blocked with 2% normal goat serum and 0.02% BSA. The cells were then incubated with 0.5 μg/mL of the primary antibodies overnight at 4°C, and the nuclei were counterstained with Hoechst. Images were scanned and analyzed using a FLUOVIEW FV3000 microscope (OLYMPUS).

ELISA

The IL-12 levels (Biolenged, 433607) and IFNγ levels (Biolenged, 430807) of the CM and tumor tissue homogenate were detected and quantified by an ELISA kit according to the manufacturer's instructions. The tissue was homogenized in chilled PBS buffer with proteinase inhibitors, and the supernatants were collected by centrifugation at 4°C for ELISA analysis to evaluate the cytokine levels in tumor tissue. The cytokine levels were then normalized to the weight of the total tissue.

Sirna-Mediated knockdown assay

The following target sequences (5–3') were used for siRNAs. siNC: CCTTCCGAAGTATCTCTTT; siCyba: GACUCCCAUUGAGCCUAAATT. Macrophages were transfected with siRNAs using Lipofectamine RNAiMAX (Invitrogen) according to the manufacturer's instructions, and further experiments were performed after 48 hours of siRNA transfection.

RNA-sequencing

For RNA-sequencing of in vitro cultured Mφ, RNA was extracted from cultured BMDMs with or without VBL treatments using TRIzol (Invitrogen). For RNA-sequencing of Mφ in tumor, RNA was extracted from macrophages sorted by FACS with a BD ArealIII (BD biosciences) flow cytometer using a EasySep Mouse F4/80 Positive Selection Kit (STEMCELL Technologies, 100-0659) according to manufacturer's instruction, the RNA was then extracted for RNA-sequencing. RNA-sequencing was then executed and analyzed as described previously.⁴⁵ Hisat2 V.2.0.5 was used to map paired-end reads to the mouse genome and feature Counts V.1.5.0-p3 was used to count the reads numbers mapped to each gene. The original read count was normalized, mainly for the correction of sequencing depth and p value was generated. Finally, multiple hypothesis testing was performed to obtain the Padj value. Finally, the list of differentially expressed genes were generated based on enrichment of Kyoto Encyclopedia of Genes and Genomes gene functional pathway. The raw data of RNA-sequencing are available at Sequence Read Archive (SRA accession: PRJNA934654).

Data randomization statement

All of the data collection was randomized, and animals and cell samples were randomly assigned to the various experimental groups. In addition, the experimental conditions and stimulus presentation were both randomized. However, the researchers involved in data collection and analysis were not blinded to the conditions of the experiments. No data were excluded from the analysis.

Statistics and reproducibility

The data were assumed to follow a normal distribution, but this was not formally tested. All data were analyzed using GraphPad Prism V.8.0.2.263 and were represented in the figures as mean values±SD. P values were determined by a two-tailed Student's t-test for comparing two groups, and two-way analysis of variance for multiple groups. P values were indicated with *p<0.05, **p<0.01, and ***p<0.001 on graphs. Graphs not labeled with an asterisk indicate that the differences between the test groups and the control groups were not statistically significant. 'n' in the figure legends indicates the number of biologically independent replicates. The Western blot and micrograph results were representative of three biologically independent replicates. All the results were independently repeated more than three times, yielding similar results.

Acknowledgements We thank the flow cytometry core facility and imaging core facility of the Shanghai Institute of Immunology. We used the ARRIVE1 checklist when writing our report.

Contributors Y-NW, JingW conceived and designed the experiments; Y-NW and JingW wrote the manuscript; JingW and Y-NW acquired funding; JingW administrated the project; Y-NW performed the main experiments; Y-YW, JinW, W-JB and N-JM helped with experiments. Y-NW and JingW reviewed and edited the manuscript. JingW is responsible for the overall content as guarantor.

Funding This work was supported by National Natural Science Foundation (31872737, 81822020, 92042304 to JW and 82302069 to Y-NW) and China Postdoctoral Science Foundation (2023T160425 to Y-NW).

Competing interests None declared.

Patient consent for publication Not applicable.

Ethics approval All animal experiments were approved by the Shanghai Jiao Tong University School of Medicine (No. A-2022-042).

Provenance and peer review Not commissioned; externally peer reviewed.

Data availability statement All data relevant to the study are included in the article or uploaded as online supplemental information.

Supplemental material This content has been supplied by the author(s). It has not been vetted by BMJ Publishing Group Limited (BMJ) and may not have been peer-reviewed. Any opinions or recommendations discussed are solely those of the author(s) and are not endorsed by BMJ. BMJ disclaims all liability and responsibility arising from any reliance placed on the content. Where the content includes any translated material, BMJ does not warrant the accuracy and reliability of the translations (including but not limited to local regulations, clinical guidelines, terminology, drug names and drug dosages), and is not responsible for any error and/or omissions arising from translation and adaptation or otherwise.

Open access This is an open access article distributed in accordance with the Creative Commons Attribution Non Commercial (CC BY-NC 4.0) license, which permits others to distribute, remix, adapt, build upon this work non-commercially, and license their derivative works on different terms, provided the original work is properly cited, appropriate credit is given, any changes made indicated, and the use is non-commercial. See <http://creativecommons.org/licenses/by-nc/4.0/>.

ORCID iD

Jing Wang <http://orcid.org/0000-0001-8758-1693>

REFERENCES

- Lan J, Sun L, Xu F, et al. M2 macrophage-derived exosomes promote cell migration and invasion in colon cancer. *Cancer Res* 2019;79:146–58.
- Nakamura A, Kurihara S, Takahashi D, et al. Symbiotic polyamine metabolism regulates epithelial proliferation and macrophage differentiation in the colon. *Nat Commun* 2021;12:2105.
- Chen T, Wang Y, Nan Z, et al. Interaction between macrophage extracellular traps and colon cancer cells promotes colon cancer invasion and correlates with unfavorable prognosis. *Front Immunol* 2021;12:779325.
- Xu F, Cui W-Q, Wei Y, et al. Astragaloside IV inhibits lung cancer progression and metastasis by modulating macrophage polarization through AMPK signaling. *J Exp Clin Cancer Res* 2018;37:207.
- Väyrynen JP, Haruki K, Lau MC, et al. The prognostic role of macrophage polarization in the colorectal cancer microenvironment. *Cancer Immunol Res* 2021;9:8–19.
- Qian BZ, Pollard JW. Macrophage diversity enhances tumor progression and metastasis. *Cell* 2010;141:39–51.
- Farajzadeh Valilou S, Keshavarz-Fathi M, Silvestris N, et al. The role of inflammatory cytokines and tumor associated macrophages (TAMs) in microenvironment of pancreatic cancer. *Cytokine Growth Factor Rev* 2018;39:46–61.
- Arwert EN, Harney AS, Entenberg D, et al. A unidirectional transition from migratory to perivascular macrophage is required for tumor cell intravasation. *Cell Rep* 2018;23:1239–48.
- Kitamura T, Doughty-Shenton D, Cassetta L, et al. Monocytes differentiate to immune suppressive precursors of metastasis-associated macrophages in mouse models of metastatic breast cancer. *Front Immunol* 2017;8:2004.
- Peranzoni E, Lemoine J, Vimeux L, et al. Macrophages impede CD8 T cells from reaching tumor cells and limit the efficacy of anti-PD-1 treatment. *Proc Natl Acad Sci U S A* 2018;115:E4041–50.
- Cassetta L, Kitamura T. Targeting tumor-associated macrophages as a potential strategy to enhance the response to immune checkpoint inhibitors. *Front Cell Dev Biol* 2018;6:38.
- Steidl C, Lee T, Shah SP, et al. Tumor-associated macrophages and survival in classic Hodgkin's lymphoma. *N Engl J Med* 2010;362:875–85.
- Mantovani A, Allavena P, Sica A, et al. Cancer-related inflammation. *Nature* 2008;454:436–44.
- Wynn TA, Chawla A, Pollard JW. Macrophage biology in development, homeostasis and disease. *Nature* 2013;496:445–55.
- Pozzi LAM, Maciaszek JW, Rock KL. Both dendritic cells and macrophages can stimulate naive CD8 T cells in vivo to proliferate, develop effector function, and differentiate into memory cells. *J Immunol* 2005;175:2071–81.
- Phillip JM, Wu P-H, Gilkes DM, et al. Biophysical and biomolecular determination of cellular age in humans. *Nat Biomed Eng* 2017;1:0093.
- Marklein RA, Lam J, Guvendiren M, et al. Functionally-relevant morphological profiling: a tool to assess cellular heterogeneity. *Trends Biotechnol* 2018;36:105–18.
- McWhorter FY, Wang T, Nguyen P, et al. Modulation of macrophage phenotype by cell shape. *Proc Natl Acad Sci U S A* 2013;110:17253–8.
- Rostam HM, Reynolds PM, Alexander MR, et al. Image based machine learning for identification of macrophage subsets. *Sci Rep* 2017;7:3521.
- Rodell CB, Arlauckas SP, Cuccarese MF, et al. TLR7/8-agonist-loaded nanoparticles promote the polarization of tumour-associated macrophages to enhance cancer immunotherapy. *Nat Biomed Eng* 2018;2:578–88.
- Melmed RN, Karanian PJ, Berlin RD. Control of cell volume in the J774 macrophage by microtubule disassembly and cyclic AMP. *J Cell Biol* 1981;90:761–8.
- Cao X, Li B, Chen J, et al. Effect of cabazitaxel on macrophages improves CD47-targeted Immunotherapy for triple-negative breast cancer. *J Immunother Cancer* 2021;9:e002022.
- Luengo-Blanco M, Prando C, Bustamante J, et al. Essential role of nuclear factor-kappaB for NADPH oxidase activity in normal and anhidrotic ectodermal dysplasia leukocytes. *Blood* 2008;112:1453–60.
- Feng Y-Y, Tang M, Suzuki M, et al. Essential role of NADPH oxidase-dependent production of reactive oxygen species in maintenance of sustained B cell receptor signaling and B cell proliferation. *J Immunol* 2019;202:2546–57.
- Harper AM, Dunne MJ, Segal AW. Purification of cytochrome B-245 from human neutrophils. *Biochem J* 1984;219:519–27.
- Stasia MJ. CYBA Encoding P22(Phox), the cytochrome B558 alpha polypeptide: gene structure, expression, role and physiopathology. *Gene* 2016;586:27–35.
- Zhang X, Yu L, Xu H. Lysosome calcium in ROS regulation of autophagy. *Autophagy* 2016;12:1954–5.
- Fang S, Wan X, Zou X, et al. Arsenic trioxide induces macrophage autophagy and atheroprotection by regulating ROS-dependent TFEB nuclear translocation and AKT/mTOR pathway. *Cell Death Dis* 2021;12:88.
- Li L, Sun S, Tan L, et al. Polystyrene nanoparticles reduced ROS and inhibited ferroptosis by triggering lysosome stress and TFEB nucleus translocation in a size-dependent manner. *Nano Lett* 2019;19:7781–92.
- Wong C-O, Gregory S, Hu H, et al. Lysosomal degradation is required for sustained phagocytosis of bacteria by macrophages. *Cell Host Microbe* 2017;21:719–30.
- Jordan MA, Wilson L. Microtubules as a target for anticancer drugs. *Nat Rev Cancer* 2004;4:253–65.
- Kashyap AS, Fernandez-Rodriguez L, Zhao Y, et al. GEF-H1 signaling upon microtubule destabilization is required for dendritic cell activation and specific anti-tumor responses. *Cell Rep* 2019;28:3367–80.
- Natoli M, Herzig P, Pishali Bejestani E, et al. Plinabulin, a distinct microtubule-targeting chemotherapy, promotes M1-like macrophage polarization and anti-tumor immunity. *Front Oncol* 2021;11:644608.
- Nardin A, Lefebvre M-L, Labroquère K, et al. Liposomal muramyl tripeptide phosphatidylethanolamine: targeting and activating macrophages for adjuvant treatment of osteosarcoma. *Curr Cancer Drug Targets* 2006;6:123–33.
- Locher C, Conforti R, Aymeric L, et al. Desirable cell death during anticancer chemotherapy. *Ann N Y Acad Sci* 2010;1209:99–108.
- Olson OC, Kim H, Quail DF, et al. Tumor-associated macrophages suppress the cytotoxic activity of antimitotic agents. *Cell Rep* 2017;19:101–13.
- Shree T, Olson OC, Elie BT, et al. Macrophages and cathepsin proteases blunt chemotherapeutic response in breast cancer. *Genes Dev* 2011;25:2465–79.
- Wang Y, Chen Y-Y, Gao G-B, et al. Polyphyllin D punctures hypertrophic lysosomes to reverse drug resistance of hepatocellular carcinoma by targeting acid sphingomyelinase. *Mol Ther* 2023;31:2169–87.
- Wang R, Yin C, Liu C, et al. Phenylboronic acid modification augments the lysosome escape and antitumor efficacy of a cylindrical polymer brush-based prodrug. *J Am Chem Soc* 2021;143:20927–38.

- 40 Kohchi C, Inagawa H, Nishizawa T, *et al.* ROS and innate immunity. *Anticancer Res* 2009;29:817–21.
- 41 Zhang Y, Choksi S, Chen K, *et al.* ROS play a critical role in the differentiation of alternatively activated macrophages and the occurrence of tumor-associated macrophages. *Cell Res* 2013;23:898–914.
- 42 Padgett LE, Burg AR, Lei W, *et al.* Loss of NADPH oxidase-derived superoxide Skews macrophage phenotypes to delay type 1 diabetes. *Diabetes* 2015;64:937–46.
- 43 He C, Ryan AJ, Murthy S, *et al.* Accelerated development of pulmonary fibrosis via Cu,Zn-superoxide dismutase-induced alternative activation of macrophages. *J Biol Chem* 2013;288:20745–57.
- 44 Shan M, Qin J, Jin F, *et al.* Autophagy suppresses isoprenaline-induced M2 macrophage polarization via the ROS/ERK and mTOR signaling pathway. *Free Radic Biol Med* 2017;110:432–43.
- 45 Wang Y-N, Tang Y, He Z, *et al.* Slit3 secreted from M2-like macrophages increases sympathetic activity and thermogenesis in adipose tissue. *Nat Metab* 2021;3:1536–51.
- 46 Kilkenny C, Browne WJ, Cuthill IC, *et al.* Improving bioscience research reporting: the ARRIVE guidelines for reporting animal research. *PLoS Biol* 2010;8:e1000412.